The Astrophysical Journal, 587:500–513, 2003 April 20

ENVIRONMENTAL EFFECTS ON EVOLUTION OF CLUSTER GALAXIES IN A Λ-DOMINATED COLD DARK MATTER UNIVERSE

Takashi Okamoto
Department of Physics, University of Durham, South Road, Durham DH1 3LE, England; and Yukawa Institute for Theoretical Physics, Kyoto University; Takashi.Okamoto@durham.ac.uk

and

Masahiro Nagashima
National Astronomical Observatory, Mitaka, Tokyo 181-8588, Japan; masa@th.nao.ac.jp
Received 2002 July 26; accepted 2002 December 26

ABSTRACT

We investigate environmental effects on evolution of bright cluster galaxies ($L > L_*$) in a Λ-dominated cold dark matter universe using a combination of dissipationless *N*-body simulations and a semianalytic galaxy formation model. The *N*-body simulations enable us to calculate orbits of galaxies in simulated clusters. Therefore, we can incorporate stripping of cold gas from galactic disks by ram pressure (RP) from the intracluster medium into our model. In this paper we study how ram pressure stripping (RPS) and small starburst induced by a minor merger affect colors, star formation rates (SFRs), and morphologies of cluster galaxies. These processes are new ingredients in our model and have not been studied sufficiently. We find that the RPS is not important for colors and SFRs of galaxies in the cluster core if the star formation timescale is properly chosen, because the star formation is sufficiently suppressed by consumption of the cold gas in the disks. Then observed color and SFR gradients can be reproduced without the RPS. The small starburst triggered by a minor merger hardly affects the SFRs and colors of the galaxies as well. We also examine whether these two processes can resolve the known problem that the hierarchical clustering models based on the major merger-driven bulge formation scenario predict too few galaxies of intermediate bulge-to–total luminosity ratio (B/T) in clusters. When the minor burst is taken into account, the intermediate B/T population is increased, and the observed morphology gradients in clusters are successfully reproduced. Without the minor burst, the RPS cannot increase the intermediate B/T population. On the other hand, when the minor burst is considered, the RPS also plays an important role in formation of the intermediate B/T galaxies. We present redshift evolution of morphological fractions predicted by our models. The predicted number ratios of the intermediate B/T galaxies to the bulge-dominated galaxies show nearly flat or slightly increasing trends with increasing redshift. We conclude that these trends are inevitable when bulges are formed through mergers. We discuss whether our results conflict with observationally suggested N_{S0}/N_E evolution in clusters, which is a decreasing function of redshift.

Subject headings: galaxies: clusters: general — galaxies: evolution — galaxies: formation — galaxies: halos — galaxies: interactions

1. INTRODUCTION

Rich clusters of galaxies are the most suitable laboratories to study how galaxy environments affect galaxy properties. The pioneering work by Butcher & Oemler (1978, 1984) has demonstrated that distant clusters contain a much higher fraction of blue galaxies than nearby clusters, although it has been questioned by Andreon & Ettori (1999). It has also been found that galaxy morphology is a function of its environment (Dressler 1980; Whitmore, Gilmore, & Jones 1993). The most recent advances have been made with the *Hubble Space Telescope*, which allows the morphology of distant galaxies to be directly compared to the properties of their nearby counterparts. Dressler et al. (1997) and Couch et al. (1998) have suggested that the predominant evolutionary effects are that the distant clusters have a substantial deficit of S0 systems compared to nearby clusters, and at lower luminosities they contain substantial Sc–Sd spirals, compared to the large population of dwarf spheroidals in present-day clusters, although their findings have been questioned by Andreon (1998). On the other hand, some recent studies (e.g., Abraham et al. 1996; van Dokkum et al. 1998; Balogh et al. 1999) have focused on observed trends in star formation rates (SFRs) and morphology as a function of position within a cluster. These studies have shown that there is smooth transition from a blue, disk-dominated population of galaxies in the outskirts of clusters to a red, bulge-dominated population in the cluster cores.

Many authors have suggested that the predominance of red, early-type galaxies in local clusters is the result of mechanisms that suppress star formation in high-density environments. This suppression makes galaxies within cluster cores redder and leads to a transformation of galaxy morphology. Comparison between the galaxy populations of local and distant clusters or those in cluster cores and outskirts provides a strong evidence for this scenario. This leads to the naive conclusion that the primary effect of the cluster environment is to transform luminous spiral galaxies into S0 galaxies through the suppression of their star formation.

Several mechanisms that may suppress the star formation and transform one morphological type into another have been proposed. Interactions between galaxies are one possible process to promote morphological transformation.

N-body simulations confirmed that major mergers between disk galaxies produce galaxies resembling ellipticals as merger remnants (e.g., Barnes 1996) and that accretion of small satellites onto their host spiral lead the morphology of the host spiral to S0 type (Walker, Mihos, & Hernquist 1996). The galaxy mergers trigger the "starburst"; therefore, the cold gas contained in these galaxies is exhausted in a very short time. These processes then cause the truncation of star formation. Although the bulge formation scenario by major mergers gives an excellent explanation for both colors (Kauffmann & Charlot 1998; Nagashima & Gouda 2001) and distribution of cluster elliptical galaxies (Okamoto & Nagashima 2001; Diaferio et al. 2001), the observed S0 population cannot be reproduced by only major mergers (Okamoto & Nagashima 2001; Diaferio et al. 2001). In addition, the galaxy mergers are the predominant effect before massive cluster formation, because, in clusters, the relative velocity of galaxies is too high for such mergers to be frequent (Ghigna et al. 1998; Okamoto & Habe 1999). Therefore, the galaxy merger is not promising as a key mechanism behind the Butcher-Oemler effect. Moore et al. (1996) examined the effects of rapid gravitational encounters between galaxies. This mechanism has been called "galaxy harassment" and is highly effective at transforming fainter Sc-Sd galaxies to dSph galaxies. While the galaxy harassment can account for the observed evolution of faint galaxies in clusters—the concentrated potentials of luminous Sa-Sb galaxies help to maintain their stability—the bulge-to-disk luminosity ratios (B/Ts) of these galaxies are hardly changed only by galaxy harassment (Moore et al. 1999). Nevertheless, if the truncation of star formation in these galaxies takes place, these galaxies can become objects that are similar to S0 galaxies, because the disks of Sa-Sb galaxies are substantially thickened and the spiral features are vanished by the harassment. It should be noted that the correlation between B/T and Hubble type has significant scatter (Baugh, Cole, & Frenk 1996), and there is no guarantee that this relation is applicable to cluster galaxies. Accordingly, we adopt the classification based on B/T to observed galaxies as well as to our model galaxies.

The second mechanism is the truncation of star formation through the removal of the diffuse hot gas reservoir that is confined in galactic dark halos and surrounds galaxies (Larson, Tinsley, & Caldwell 1980). In clusters, any hot diffuse material originally trapped in the potentials of the galactic halos becomes part of the overall intracluster medium (ICM). A galaxy whose hot gas reservoir is removed slowly exhausts its cold gas in a few gigayears (e.g., Gallagher, Bushouse, & Hunter 1989), because there is no supply of fresh gas from the surrounding hot gas. This process is an important ingredient in the success of semianalytic (SA) models, which have been shown to reproduce observed global properties of cluster galaxies such as the morphological composition and the blue galaxy fraction (e.g., Baugh et al. 1996; Kauffmann 1996). Although such slow truncation after the infall into larger virialized halos explains the observed SFR gradients in clusters (Balogh, Navarro, & Morris 2000) and the color evolution of cluster galaxies (Kodama & Bower 2001), the lack of a population of intermediate B/T cannot be solved even by including this mechanism into the galaxy formation model (Diaferio et al. 2001).

The other mechanism is ram pressure stripping (RPS) of the cold gas from galactic disks (Gunn & Gott 1972). As a galaxy orbits through a cluster, it experiences ram pressure (RP) from the ICM. When the RP is greater than the binding force, the cold gas will be stripped in $\sim 10^7$ yr (Abadi, Moore, & Bower 1999). Fujita & Nagashima (1999) suggested that the RPS increases B/T of the Milky Way–like galaxies because of the rapid suppression of the star formation in the disk component, and consequently Sb galaxies change their morphology into S0 galaxies by assuming static cluster potentials and radially infalling galaxies.

In this paper we investigate how these mechanisms affect colors and morphologies of cluster galaxies with a special interest in the effects of the RPS and the minor mergers that have not been well studied in cosmological context. Here we do not attempt to model the galaxy harassment because we treat only bright galaxies ($L > L_*$), and the galaxy harassment probably does not affect strongly for such bright galaxies as far as we classify the galaxies by B/T, as we mentioned previously.

For this purpose, the fully numerical simulations are still too expensive and have a lot of difficulty in handling "subgrid" physics, e.g., gas cooling, star formation, supernova feedback, chemical evolution, and so on; however, recent work is beginning to achieve some notable successes for the distribution of galaxy populations (e.g., Steinmetz & Müller 1995; Weinberg, Hernquist, & Katz 1997; Blanton et al. 1999; Katz, Hernquist, & Weinberg 1999; Pearce et al. 1999; Cen & Ostriker 2000).

An alternative method to study the evolution of galaxy population is the SA modeling of galaxy formation (e.g., Kauffmann, White, & Guiderdoni 1993; Cole et al. 1994, 2000; Somerville & Primack 1999; Nagashima et al. 2001, 2002), which follows the collapse and merging of dark halos by using a probabilistic method on the mass distribution based upon an extension of the Press-Schechter formalism (Press & Schechter 1974; Bond et al. 1991; Bower 1991; Lacey & Cole 1993) and in which the subgrid physics is incorporated with the merging histories of dark matter halos assuming simple scaling laws.

As a natural expansion of this approach, hybrid methods of cosmological *N*-body simulations and the phenomenological model of galaxy formation used in the SA techniques have been developed (Roukema et al. 1997; Kauffmann et al. 1999; Benson et al. 2000). In order to obtain the spatial and velocity distribution of galaxies and to treat the mergers between galaxies in the cluster environment, several authors have adapted the refinements of hybrid methods, which traces the merging histories of substructures within virialized halos (Okamoto & Nagashima 2001; Springel et al. 2001). Since this method enables us to calculate orbits of galaxies in clusters, we can incorporate the RPS in our model as well as the merging of substructure halos.

We compare our simulated cluster at $z = 0.2$ to an observed sample that is constructed by superposing seven low-redshift CNOC1 clusters ($0.18 < z < 0.3$; see Yee, Ellingson, & Carlberg 1996). To compare our results with the observations, we rescale our simulated cluster and the CNOC1 clusters by R_{200}, which is the radius of the sphere centered on the cluster center and whose density is 200 times the critical density of the universe at a given redshift.

In § 2, we describe an outline of the galaxy formation model used here, and we show the characteristics of our model in § 3. Results for the luminosity functions, star formation gradients, color gradients, and morphological gradients are presented in § 4. The results are discussed in § 5.

2. MODEL

We examine the evolution of cluster galaxies in a Λ-dominated cold dark matter universe ($\Omega_0 = 0.3$, $\lambda_0 \equiv \Lambda_0/(3H_0^2) = 0.7$, $h \equiv H_0/100$ km s^{-1} Mpc$^{-1} = 0.7$, $\sigma_8 = 1.0$). The baryon density Ω_b is set to 0.015 h^{-2} (Suzuki, Yoshii, & Beers 2000). Note that a recent measurement of the anisotropy of the cosmic microwave background suggests a slightly higher value, $\Omega_b \simeq 0.02\ h^{-2}$ (Netterfield et al. 2002). The changing of Ω_b affects only the normalization of parameters in our SA model, and we confirmed that it does not affect our conclusion. Thus, here we prefer using $\Omega_b = 0.015\ h^{-2}$, which was adopted in our previous paper (Okamoto & Nagashima 2001).

The outline of the procedures of galaxy formation is as follows. At first, the merging paths of dark halos are realized by a cosmological N-body simulation. At this stage, it is determined for each halo whether it is a central halo of its virialized host halo or it is a substructure of its host. Next, in each merging path, evolution of the baryonic components, namely, gas cooling, star formation, supernova feedback, and chemical evolution, are calculated based on the SA galaxy formation model. The detail of our SA model will be given in § 2.3.

We refer to a system consisting of the stars and cold gas as a "galaxy." When two or more galactic halos merge together, we estimate the merging timescale of the galaxies in the new common halo based on a dynamical friction timescale. As merging of galaxies occurs, we change the morphology of the merger remnant according to the type of the merger. Finally, we calculate the luminosity and color of each galaxy based on the stellar populations that comprise the galaxy.

2.1. *Simulations*

We first describe two simulations used in this paper and their specific purpose. These simulations are the same as those by Okamoto & Habe (1999, 2000) except for the background cosmology.

For a main simulation, we adopt the constrained random field method to generate the initial density field, in which a rich cluster is formed at the center of a simulation sphere of radius 22.5 h^{-1} Mpc (Hoffman & Ribak 1991). The constraint that we impose is the 3 σ peak with the 8 Mpc Gaussian smoothed density field at the center of the simulation sphere. We refer to this simulation as the "cluster simulation."

Another simulation represents an average piece of the universe corresponding to the "field" environment within a sphere of radius 20 h^{-1} Mpc without any constraints. We use this simulation to normalize the parameters in our galaxy formation models and to compare the galaxy population to that in the cluster simulation. Although the size of this simulation seems to be somewhat small, Okamoto & Habe (1999) obtained a reasonable halo mass function from a simulation sphere of radius 3.5 h^{-1} Mpc. We have confirmed that this simulation produces a reasonable mass function, and the mass of the most massive halo at $z = 0$ is sufficiently small ($1.9 \times 10^{13}\ M_\odot$) as a sample of low-density environment.

To get sufficient resolution with relatively small number of particles, we use a multimass initial condition for each simulation. In the field simulation, we put the high-resolution particles in the sphere of radius 10 h^{-1} Mpc, and in the remaining region we put the low-resolution particles as boundary particles. On the other hand, we adopt the resimulation technique for the cluster simulation (Okamoto & Habe 1999). That is, first only long-wavelength components are used for the realization of the initial perturbations in the simulation sphere using $\sim 10^5$ particles, and then we perform a simulation with these low-resolution particles. After this procedure, we tag the particles that are inside the sphere of radius 3 h^{-1} Mpc centered on the cluster center at $z = 0$. Next we go back to the initial redshift, and then we divide the tagged particles according to the density perturbations that is produced by additional shorter wavelength components. As a result, the number of high-resolution particles becomes $\sim 10^6$. We adopt the same mass and softening length of a high-resolution particle in each simulation. Our analyses are operated only for these high-resolution particles.

The overall parameters and mass of the most massive virialized object in each simulation at $z = 0$ are listed in Table 1.

2.2. *Halo Identification and Construction of Merger Trees*

The method to create merging history trees of dark halos is basically the same as Okamoto & Habe (2000), to which we make some improvement. To construct the merger trees we identify virialized halos and their substructures at 34 redshifts during $z = 20$ and $z = 0$. This procedure is as follows.

At each time step, we calculate the density field by smoothing each particle with 64 neighboring particles using a similar method to the smoothed particle hydrodynamics (SPH). At a given redshift, particles with local densities greater than $\frac{1}{3}$ of the virial density at that redshift are tagged.

We then operate the friends-of-friends (FOF) grouping algorithm (Davis et al. 1985) on only the tagged particles; otherwise, the FOF is likely to find strangely shaped halos like strings in low-density regions (Bertschinger & Gelb 1991). The linking length is defined as $b\bar{l}$, where $\bar{l}$ is the mean particle separation and the parameter b is a function of redshift. Its value is given by

$$b = \left(\frac{1}{2}\frac{\rho_{\rm vir}}{\bar{\rho}}\right)^{-1/3}, \qquad (1)$$

TABLE 1
PARAMETERS OF SIMULATIONS

Simulation	Constraint	N_h	N_l	ϵ_h	ϵ_l	m_h	m_l	$R_{\rm sim}$	$M_{\rm largest}$
Field	None	636,008	824,438	5E−3	2E−2	5.5E+8	4.4E+9	20	1.87E+13
Cluster	3 σ peak	1121,534	95,406	5E−3	5E−2	5.5E+8	3.5E+10	22.5	5.23E+14

NOTES.—Parameters N, ϵ, m, $R_{\rm sim}$, and $M_{\rm largest}$ represent number of particles in each simulation, mass of a particle, radius of each simulation sphere, and mass of the largest virialized object in each simulation at $z = 0$, respectively. Subscripts h and l indicate high-resolution and low-resolution particles, respectively. A length unit is h^{-1} Mpc and a mass unit is $h^{-1}\ M_\odot$.

where $\rho_{\rm vir}$ is the virial density calculated by the spherical collapse model at a given redshift and $\bar{\rho}$ is the background density of the universe. Note that equation (1) implies the density of a halo edge is half of the virial density, which well exceeds the criterion used to tag the particles. This equation gives $b \simeq 0.2$ when we assume 200 as the virial overdensity, which is often used in the case of the critical density universe. When the FOF links more than 10 tagged particles, we identify this linked particle group as a virialized object. We call the halos found by this procedure "FOF halos."

Next, we divide these FOF halos into substructures according to their density peaks. For this purpose, we use the SKID algorithm (Governato et al. 1997) as a substructure finder. The particles contained in the FOF halos are moved along the density gradients to the local density maxima. At each density peak, the localized particles are grouped. After we remove the gravitationally unbound particles in each group, we identify the groups that contain more than 10 particles as substructures. We call these groups "SKID halos." The SKID halo that contains the most bound particles of its host FOF halo is defined as a central SKID halo, and its properties are replaced by those of the host FOF halo. In Figure 1, we show the density map of the cluster at $z = 0$ and the particles contained in the FOF halos and the SKID halos.

The merger tree of each SKID halo is constructed by the method described by Okamoto & Habe (2000). Note that we trace halo stripped galaxies as well as the SKID halos using the most bound particle in a SKID halo as a tracer particle (see Okamoto & Habe 1999, 2000).

Since cooling is not allowed in substructure halos (i.e., noncentral SKID halos) in our model as we describe in § 2.3.2, the noncentral SKID halos that do not have any progenitors at a previous time step cannot contain either stellar or cold gas components. Thus, we remove these useless SKID halos from our merger trees. As a result, a newly formed SKID halo, i.e., a SKID halo that has no progenitor at previous time step, is always born as a central SKID halo.

2.3. *Galaxy Formation Model*

The following prescriptions are almost the same as the model in Okamoto & Nagashima (2001). For simplicity, a dark halo is modeled as a truncated isothermal sphere whose mass and circular velocity are taken from the N-body data. If a dark matter halo has no progenitor halos, the mass fraction of the gas is given by $f_b = \Omega_b/\Omega_0 \simeq 0.1$. When a dark matter halo collapses, the gas in the halo is shock-heated to the virial temperature of the halo. We refer to this heated gas as "hot gas." The gas in the dense region of the halo is cooled by efficient radiative cooling. We dub this cooled gas "cold gas." We estimate the amount of the gas cooled during a time step using the metallicity-dependent cooling function by Sutherland & Dopita (1993). In order to avoid the formation of unphysically large galaxies, the above cooling process is applied only to halos with circular velocities smaller than $V_{\rm stop}$. When we adopt the same value of $V_{\rm stop}$ for the field and cluster simulations, our simulations produce too many/few bright galaxies in the field/cluster simulation. Although this discrepancy is interesting, our simulations are too small to argue the bright end of luminosity functions, and it is beyond the scope of this paper. Moreover, the physical meaning of $V_{\rm stop}$ is quite unclear. Therefore, we choose the values of $V_{\rm stop}$ to reproduce the observed number of bright galaxies ($L > L_*$). We adopt $V_{\rm stop} = 350$ and 500 km s^{-1} for the filed and cluster simulations, respectively.

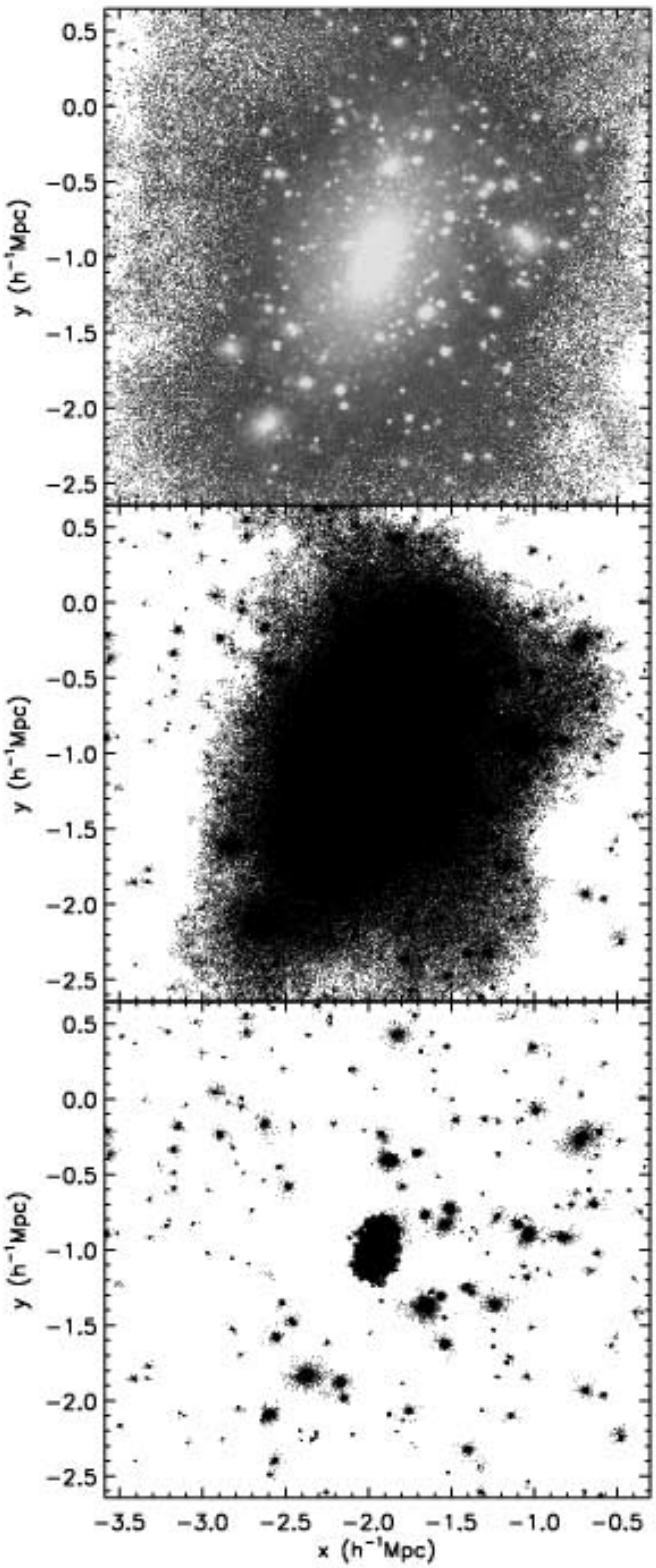

FIG. 1.—Density map (*top panel*), the x-y projection of the particles contained in FOF halos (*middle panel*), and projection of those in SKID halos (*bottom panel*) within the cluster's virial radius at $z = 0$.

Stars are formed from the cold gas at a rate of $\dot{M}_* = M_{\rm cold}/\tau_*$, where $M_{\rm cold}$ is the mass of the cold gas and τ_* is the star formation timescale in the disk. It means that the cold gas in the disk is consumed in about τ_* if there is not any supply of the fresh gas.

When the star formation timescale is a function of redshift as in the case of $\tau_* \propto \tau_{\rm dyn}$, where $\tau_{\rm dyn}$ is the dynamical time of a galaxy, the observed properties of the high-redshift galaxies cannot be reproduced (Kauffmann & Haehnelt 2000; Somerville, Primack, & Faber 2001; Nagashima et al. 2001). We then adopt the description by Cole et al. (1994),

$$\tau_* = \tau_*^0 \left(\frac{V_c}{300 \text{ km s}^{-1}} \right)^{\alpha *} , \quad (2)$$

where τ_*^0 and α_* are free parameters. These free parameters are fixed by matching the observed mass fraction of the cold gas in neutral form in the disks of spiral galaxies.

In our model, stars with masses larger than 10 $M_\odot$ explode as Type II supernovae (SNe II) and heat up the surrounding cold gas. This SN feedback reheats the cold gas to the hot phase at a rate of $\dot{M}_{\rm reheat} = M_{\rm cold}/\tau_{\rm reheat}$, where the timescale of reheating is given by

$$\tau_{\rm reheat} = (V_c/V_{\rm hot})^{\alpha_{\rm hot}} \tau_* , \quad (3)$$

where $V_{\rm hot}$ and $\alpha_{\rm hot}$ are free parameters. Although they are to be determined by matching the local luminosity function of galaxies, we set $\alpha_{\rm hot}$ to 2.0 because changing this value has a minimal effect on the results if we determine other parameters to reproduce observations of local galaxies.

Chemical evolution is treated in almost the same way as described in Kauffmann & Charlot (1998). The instantaneous recycling approximation is adopted. We assume that the initial gas has a primordial composition (zero metallicity). Then the gas is polluted by SNe II. The amount of metals ejected from SNe is characterized by y, which is the heavy element yield for each generation of stars. The value is defined by matching the color-magnitude relation (CMR) of the local cluster elliptical galaxies, and we adopt $y = 3\ Z_\odot$ in this paper. All the ejecta is incorporated with the cold gas, while 30% of the ejecta was assumed to be directly expelled to the hot gas in Kauffmann & Charlot (1998). The gas fraction returned by evolved stars is 0.25 in this paper. Simultaneously, the SNe heat up the surrounding cold gas, and then metals contained in the cold gas are also returned to the hot gas. The returned metals affect the cooling rate of the hot gas, and the cooling transfers the metals from the hot gas to the cold gas.

Before we describe our merging procedure, let us explain our galaxy hierarchy. As we mentioned before, FOF halos represent virialized dark halos. Each FOF halo hosts one central SKID halo along with a number of noncentral SKID halos that represent substructures of the FOF halo. Each SKID halo hosts one central galaxy along with a number of satellite galaxies. As we describe § 2.3.2, only the central galaxy in the central SKID halo can be supplied with the fresh cold gas by radiative cooling. The merging between SKID halos are directly obtained from N-body simulations. Here we consider the merging between galaxies within a SKID halo.

When two or more SKID halos have merged, we identify a central galaxy of the largest progenitor as a central galaxy of the new common SKID halo. Other galaxies are regarded as satellite galaxies. For simplicity, we take account of only the merging between a satellite galaxy and the central galaxy. A satellite galaxy falls into the central galaxy in a dynamical friction timescale,

$$\tau_{\rm mrg} = \frac{1}{2} \frac{f(\epsilon)}{C} \frac{V_c r_{\rm halo}^2}{G M_{\rm sat} \ln \Lambda_{\rm C}} , \quad (4)$$

where $r_{\rm halo}$ and V_c are the radius and circular velocity of the new common halo, respectively, $M_{\rm sat}$ is the mass of the satellite, and $\ln \Lambda_{\rm C}$ is the Coulomb logarithm. If the satellite has a halo at a previous time step, $M_{\rm sat}$ is defined as the mass of the SKID halo to which the satellite belongs as the central galaxy at the previous time step. Since we trace halo-stripped galaxies as well, the mass composed by stars and cold gas is used as $M_{\rm sat}$ when the satellite does not have a halo at a previous time step. The function $f(\epsilon)$ describes the dependence of the orbital decay on the eccentricity of the orbit, expressed in terms of $\epsilon = J/J_c(E)$, where $J_c(E)$ is the angular momentum of a circular orbit with the same energy as the satellite. This function is well approximated by $f(\epsilon) \simeq \epsilon^{0.78}$, for $\epsilon > 0.02$ (Lacey & Cole 1993). C is a constant with value $\simeq 0.43$. For $f(\epsilon)$, we adopt the average value, $\langle f(\epsilon) \rangle \simeq 0.5$, computed by Tormen (1997).

When a satellite galaxy merges with a central galaxy and the mass ratio of the satellite to the central galaxy is larger than $f_{\rm major}$, we regard this merger as a major merger, and then all stars of the satellite and disk stars of the central galaxy are incorporated with the bulge of the central galaxy. At the same time, cold gas contained in both galaxies is consumed to form bulge stars by starburst with the same feedback law as in the disk star formation.

If the mass ratio does not exceed the value of the parameter $f_{\rm major}$, the merger is classified as minor. When we adopt the standard prescription, in the case of the minor merger, the disk of the central galaxy is preserved, no starburst takes place, and the stars from the satellites are added to the bulge of the central galaxy.

In this paper we also consider the case that a minor merger triggers a small starburst because numerical experiments of merging galaxies have suggested that a starburst is induced by a minor merger as well as a major merger (Walker et al. 1996). We dub this process the "minor burst" and give a detailed prescription in § 2.3.1.

In this paper, we adopt $f_{\rm major} = 0.2$ that was used for the low-density universe in Okamoto & Nagashima (2001). We confirmed that our results hardly depend on $f_{\rm major}$, since our morphological classification based on B/T is normalized to reproduce the observed morphological composition in the field.

The absolute luminosities and colors of individual galaxies are calculated using a population synthesis model by Kodama & Arimoto (1997). The initial stellar mass function (IMF) that we adopt is the power-law IMF of Salpeter form with lower and upper mass limits of 0.1 and 60 $M_\odot$, respectively.

As we stated above, we divided the stellar component into disk and bulge components. In the previous SA studies, morphology of each galaxies has been determined by the B-band B/T. Simien & de Vaucouleurs (1986) showed that the Hubble types T of galaxies correlated with B/T by following the relation

$$\langle \Delta M \rangle = 0.324(T+5) - 0.054(T+5)^2 + 0.0047(T+5)^3 , \quad (5)$$

where $\Delta M \equiv M_B^{\rm bulge} - M_B^{\rm total}$. In this paper we use this relation to assign the Hubble type to our model galaxies. Unfortunately, this relation has significant scatter (Baugh et al. 1996); therefore, we prefer direct comparison of B/Ts of the model galaxies with those of the observed galaxies as we describe in § 4.4.

2.3.1. *Starburst Triggered by a Minor Merger*

The effect of minor mergers was studied in Mihos & Hernquist (1994) using SPH simulations including star formation. In the case of a merger between a Milky Way–sized disk galaxy and a satellite with total mass equal to 10% of the central disk galaxy mass, the bar instability leads to gas fueling the galactic center; thus, 50% of the total gas is consumed in the starburst. If the central galaxy has a bulge, the bulge stabilizes the disk and prevents the gas fueling. When the bulge-to-disk mass ratio is larger than $\frac{1}{3}$, the starburst becomes negligible.

Somerville et al. (2001) modeled this process by assuming that the fraction of cold gas consumed by the starburst is a function of the merging mass ratio. However, since only a limited parameter range has been explored, how the starburst efficiency depends on the mass ratio is highly unknown. Moreover, the starburst during a violent merger and the starburst triggered by the bar instability should be treated separately. Then we model the minor burst by assuming that the fraction $f_{\rm burst}$, of the cold gas is consumed by the minor burst when the merger mass ratio is between $f_{\rm minor}$ and $f_{\rm major}$ for simplicity. In the case of the minor burst, the stellar disk of the central galaxy is preserved. When the bulge-to-disk mass ratio of the central galaxy is larger than $\frac{1}{3}$, the minor burst does not take place according to Mihos & Hernquist (1994). We set these two parameters to reproduce the morphology-radius relation ($f_{\rm burst} = 0.25$ and $f_{\rm minor} = 0.1 f_{\rm major}$), as we show in § 4.4.

Note that if we adopt $f_{\rm burst} = 1$, it provides very similar results to the model without the minor burst and with small $f_{\rm major}$ ($\simeq f_{\rm minor}$) in clusters, because most of the gas is consumed by the mergers at high redshifts in any case. The model with small $f_{\rm major}$ only increases the bulge-dominated fraction and does not increase the intermediate B/T fraction (Okamoto & Nagashima 2001).

2.3.2. *Stripping of Diffuse Hot Gas*

We include the stripping of diffuse hot gas from galactic halos in our modeling as follows. When a FOF halo contains more than two SKID halos, the properties of the central SKID halo are replaced with those of the host FOF halo as we mentioned in § 2.2. The hot gas contained in the noncentral SKID halos are simply added to the hot gas reservoir of the host FOF halo (i.e., the central SKID halo), so only the central galaxy in the central SKID halo can be supplied with the fresh cold gas by radiative cooling. This process has already been included in the previous SA studies and led to significant success (e.g., Baugh et al. 1996; Kauffmann & Charlot 1998; Diaferio et al. 2001).

2.3.3. *Ram Pressure Stripping of Cold Gas Disk*

The RPS of cold disk gas is also a new ingredient of our model. By following the simple method, we estimate stripping effects of cold gas by RP from an ICM.

In order to estimate the strength of the RP, we need to know the orbits of cluster galaxies. For this purpose, we assume that the cluster has an NFW (Navarro, Frenk, & White 1997) type of density distribution, and then we fit the density profile of the main cluster (i.e., the most massive virialized object) at each time step of the merging history by the NFW profile,

$$\rho(r) = \frac{\rho_0}{(r/r_s)(1 + r/r_s)^2} \ , \tag{6}$$

where ρ_0 and r_s are fitting parameters. Once we fit the density profile of a cluster, we can calculate the potential energy as a function of the distance from the cluster center,

$$\Psi(r) = -4\pi r_s^2 G\rho_0 \frac{\ln(1 + r/r_s)}{r/r_s} - \frac{1}{2} H_0^2 \lambda_0 r^2 \ . \tag{7}$$

Then we calculate the orbits of the galaxies within $2R_{\rm vir}$ from the center of the main cluster using their positions and relative velocities to the cluster.

Although gradual removal is preferable, we consider here only instantaneous stripping as a maximal effect because we have to output data with a quite small time step to achieve the gradual removal of gas, and such a treatment is not practical. Thus, the RP is estimated at pericentric positions for outgoing galaxies and at present positions for ingoing galaxies. This treatment avoids too early stripping for the ingoing galaxies that do not pass the pericentric positions during the time step.

The RP from the ICM is estimated as follows at the stripping positions:

$$P_{\rm ram} = \rho_{\rm ICM} v_{\rm gal}^2 \ , \tag{8}$$

where $\rho_{\rm ICM}$ is the density of the ICM and $v_{\rm gal}$ is the velocity of a galaxy relative to the ICM. We suppose that the ICM distributes parallel to the dark matter for simplicity. The density of the ICM is obtained as $f_b\rho(r)$, where $\rho(r)$ is taken from the NFW fit. The hot gas fraction in the main halo at $z < 1$ is $\sim$0.75; however, using $0.75 f_b \rho(r)$ as $\rho_{\rm ICM}$ makes no visible difference. Thus, we assume the hot gas fraction is unity for simplicity.

We also attempted the ICM distribution that has the Coma-like core with the core density, $\rho_c = 7.98 \times 10^{-27} h^{1/2}$ g cm^{-3} (Briel, Henry, & Böhringer 1992) by putting the ceiling to the density distribution. With the above choice of the core density, the core radius becomes $r_c \simeq 140\ h^{-1}$ kpc ($\sim 0.12 R_{200}$) at $z = 0.2$. This radius is much smaller than the radius at which the effect of the RPS becomes significant as we show in § 4.2, and then we cannot find any difference in the results from the coreless distribution. Therefore, we show only the results in the case of the ICM distribution parallelized to dark matter.

For the cold gas, the restoring force per unit area owing to the gravity of the galactic disk is given by

$$F_{\rm grav,\,cold} = 2\pi G \Sigma_{*,\,\rm disk} \Sigma_{\rm cold} \ , \tag{9}$$

where $\Sigma_{*,\rm disk}$ is the surface density of the stellar disk and $\Sigma_{\rm cold}$ is that of the cold gas (Gunn & Gott 1972). We calculate $\Sigma_{*,\rm disk}$ as $0.5 M_{*,\rm disk}/\pi r_e^2$, where r_e is an effective radius of the disk assuming that the effective radius is identical to the half-mass radius of the disk. The effective radius is given by matching the observed luminosity-radius relation of spiral galaxies (see § 3.1). Assuming $\Sigma_{\rm cold} \propto \Sigma_{*,\rm disk}$, the surface density of the cold gas is given by $\Sigma_{\rm cold} = (M_{\rm cold}/M_{*,\rm disk})\ \Sigma_{*,\rm disk}$.

Since we consider the maximal effect of the RPS, we suppose that all cold gas in a disk is stripped when $P_{\rm ram} > F_{\rm grav}$. The stripped cold gas is mixed with the hot gas of the host FOF halo.

3. MODEL SETS

In this paper we investigate the following four baseline models and their combinations to clarify effect of each process. As the standard prescription of SA models, we consider the model without either the RPS or the minor burst. By this model we define a reference parameter so that this model reproduces the properties of the local galaxies. The model with the reference parameter set is called the "standard" model. When no fresh cold gas is supplied, the cold gas in a galaxy is exhausted by the star formation, and then the star formation is truncated. Since this truncation timescale is determined by the star formation timescale τ_*, we also consider a model with longer star formation timescale than the standard model. The model with the star formation timescale that is 4 times as long as the standard one is referred to as the "low SFR" model. The model with the minor burst and the model with the RPS are called the "minor burst" model and the "RPS" model, respectively. In these models, the reference parameter set is used.

All models are studied in both the cluster and field simulations except for the RPS model, which is unimportant in the field. Thus, the corresponding model to the cluster standard and the RPS models in the field is the field standard model. When we compare the cluster simulation to the field simulation, we always use the corresponding field model, for example, the minor burst model in the field for the minor burst model in the cluster and the low SFR model in the field for the low SFR+RPS model in the cluster. These models are simply dubbed the "field" models.

3.1. *Parameter Setting*

In this subsection we show characteristics of our models and how each process affects the properties of the local field galaxies. The values of the parameters used in the standard model are listed in Table 2.

In the top panel of Figure 2 we show the model *B*-band luminosity functions in the field at $z = 0$ and the observed one taken from APM (Loveday et al. 1992), ESP (Zucca et al. 1997), UKST (Ratcliffe et al. 1998), and 2dF (Folkes et al. 1999).

Since the simulation volume for the field is too small, the brightest bin in the standard model contains only two galaxies. Therefore, we do not attempt to reproduce the bright end of the field luminosity function in this paper.

Apart from the bright end, our luminosity functions are smaller at the intermediate luminosity range than those in the observations, and their slopes at faint ends are steeper than observed slopes. This difference may cancel out if random collisions between satellite galaxies (in substructure halos) are considered (Somerville & Primack 1999) or if we use higher resolution that enables us to identify dark halos of smaller satellite galaxies (Springel et al. 2001).

It is found that the minor burst hardly affects the galaxy luminosity function, at least in the field. The luminosity functions in the standard and minor burst models almost overlap. The effect of the star formation timescale is also small as shown in Cole et al. (2000).

TABLE 2
PARAMETERS OF GALAXY FORMATION MODEL

Parameter	Value
$V_{\rm hot}$ (km s^{-1})	200
$\alpha_{\rm hot}$	2.0
τ_*^0 (Gyr)	2.0
α_*	−1.3
$f_{\rm major}$	0.2
$y\,(Z_\odot)$.....	3.0

Although a model luminosity function is very sensitive to the choice of the feedback parameters ($V_{\rm hot}$, $\alpha_{\rm hot}$) and the circular velocity above which the cooling is stopped ($V_{\rm stop}$), we note that the shape of the luminosity function does not have particular importance for our results. The key observa-

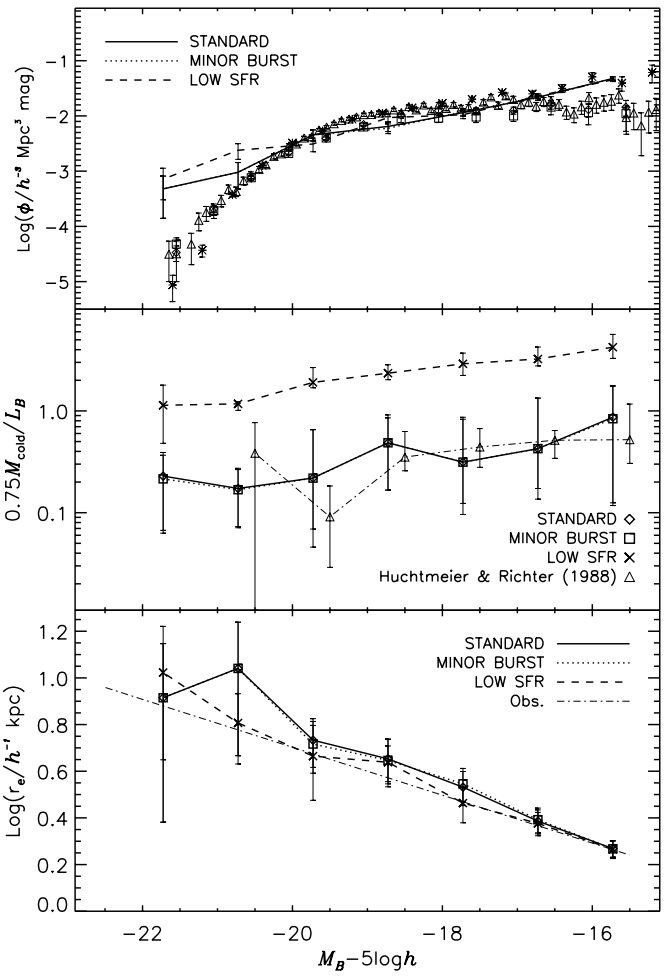

FIG. 2.—Properties of the galaxies in the field models as a function of *B*-band luminosity. *B*-band luminosity functions, cold gas mass fractions in spiral galaxies, and size of spiral galaxies are presented in the top, middle, and bottom panels, respectively. The solid, dotted, and dashed lines indicate the standard, minor burst, and low SFR models, respectively. The observed data are represented by symbols for the luminosity functions (squares, asterisks, diamonds, and triangles for APM, ESP, UKST, and 2dF, respectively) and dash-dotted lines for the cold gas mass fractions and the galaxy size. The details are given in the text.

tional constraints in this paper are the number of bright galaxies ($L > L_*$), the cold gas mass fraction in a late type galaxy, and the disk size. The number of bright galaxies are controlled by $V_{\rm stop}$, and the latter two are used to specify our model parameters as described below.

When examining the effects of gas stripping, one of the most important quantities is the cold gas fraction in galaxies that reside in the environment where the stripping effects are negligible. The cold gas content of galaxies are strongly affected by the star formation parameters τ_*^0 and α_* (Cole et al. 2000). In the middle panel of Figure 2 we show the cold hydrogen fraction of the spiral and irregular galaxies in the field models. The observational data are taken from the H I observation by Huchtmeier & Richter (1988), which come from a complete sample of the galaxies with morphological type $T \geq 1$. We classify our galaxy according to equation (5) and choose the galaxy with $T \geq 1$. It is found that the models with the reference parameter set reproduce the observation well. There is no difference between the standard model and the minor burst model again. The fraction in the low SFR model is much larger than that in the standard model and the observation as expected.

Another important quantity when we argue the RPS is the size of a disk that is used to calculate the surface density of the disk. We assume that the disk size is proportional to the virial radius of its host halo. In the bottom panel of Figure 2 we show the case that r_e is 5% of the virial radius. We also show the observed best-fit relation given by Totani & Yoshii (2000) for the data in Impey et al. (1996). It is found that our model gives a good agreement with the observed relation.

One important conclusion in this subsection is that the minor burst hardly affects the properties of the field galaxies with our values of $f_{\rm minor}$ and $f_{\rm burst}$ at least at $z = 0$.

4. RESULTS

4.1. *Global Properties*

Before we investigate the distribution of galaxy population, it is worthwhile looking over global properties of our cluster galaxies.

In Figure 3, we show B-band luminosity functions of cluster galaxies in the standard, low SFR, and minor burst models and their combination with the RPS at $z = 0$. We also show the observed luminosity function in the Virgo Cluster (Sandage, Binggeli, & Tammann 1985). All models broadly agree with the observation. The luminosity function in the low SFR model is always larger than those in other models because B-band luminosity reflects recent star formation. The RPS affects only the low SFR model significantly, especially at the faint end, because the galaxies in this model have more cold gas than those in the models with the standard star formation timescale and the cold gas in the faint galaxies are easily stripped.

To see effects of truncation of star formation on colors of galaxies, in Figure 4 we show CMRs for all types of galaxies in the standard field model and galaxies within cluster cores ($r < 0.5\ h^{-1}$ Mpc) in the standard, RPS, minor burst, low SFR, and low SFR+RPS models. We do not show the minor burst+RPS model because it is quite similar to the RPS model. Here we classify the galaxies with $T < 0.92$ according to equation (5) as early-type galaxies (*diamonds*) and others as late-type galaxies (*plus signs*). The observed

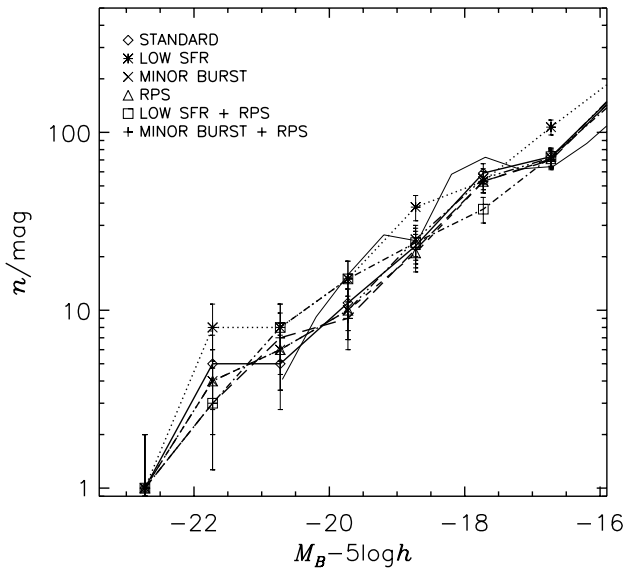

FIG. 3.—*B*-band luminosity functions of cluster galaxies. The diamonds, asterisks, crosses, triangles, squares, and pluses indicate the luminosity functions of the standard, low SFR, minor burst, RPS, low SFR+RPS, and minor burst+RPS models, respectively. The thin solid line is the luminosity function of the Virgo Cluster of galaxies by Sandage et al. (1985).

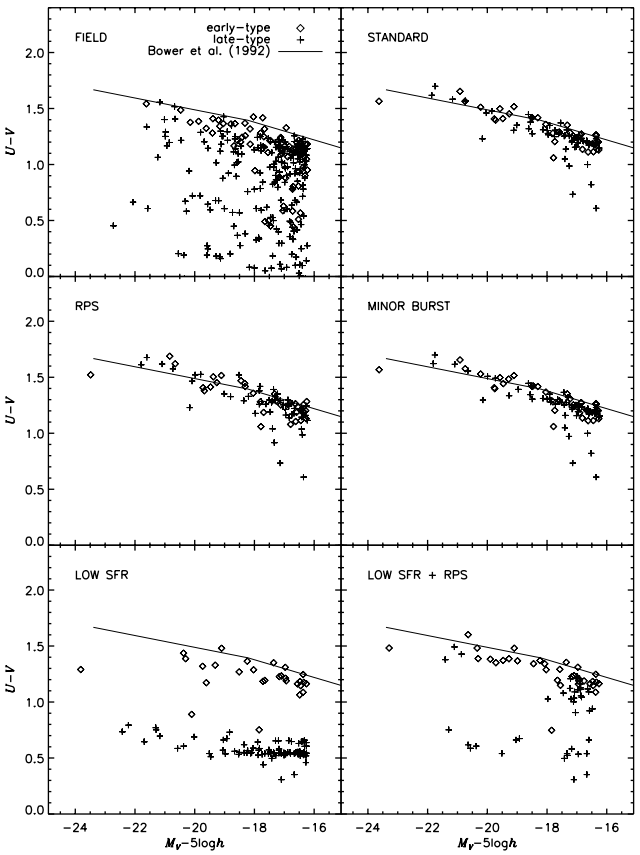

FIG. 4.—Color-magnitude diagrams at $z = 0$. We show $U-V$ colors of galaxies in the field model (*top left*) and galaxies within the cluster core in the standard (*top right*), RPS (*middle left*), minor burst (*middle right*), low SFR (*bottom left*), and low SFR+RPS (*bottom right*) models as a function of V-band luminosity. Galaxies with $T < 0.92$ by eq. (5) are classified as early-type galaxies (*diamonds*), and other galaxies are classified as late-type galaxies (*plus signs*). The solid lines show the observed CMR for cluster elliptical galaxies by Bower et al. (1992), which are applied aperture correction (Kodama et al. 1998).

CMR for the Coma elliptical galaxies is indicated by solid lines (Bower, Lucy, & Ellis 1992), which is the applied aperture correction (Kodama et al. 1998). In the models with the proper star formation timescale (standard, RPS, and minor burst), the blue population seen in the field model vanishes, and then the galaxies distribute within ± 2 mag from the CMR for the observed cluster elliptical galaxies as observed in the Coma Cluster (Terlevich, Caldwell, & Bower 2001). This is caused by the hot gas stripping in the standard model. The earlier formation epochs of galactic halos in the cluster environment may not be important for this because the late-type galaxies in the low SFR model have significantly bluer colors than the standard model. On the other hand, the CMRs for early-type galaxies are quite similar in all models, even in the field. It suggests that the main star formation truncation mechanism for the early-type galaxies is the starburst caused by the major merger.

Since the star formation is sufficiently suppressed in the standard model, the significant difference by the RPS is only seen between the low SFR model and the low SFR+RPS model. However, even in the low SFR+RPS model, there are a lot of too blue galaxies. Thus, we conclude that the most important star formation truncation mechanism for the disk-dominated galaxies in cluster cores is the hot gas stripping. We cannot see any significant effect by the minor burst on the CMR.

4.2. *SFR Gradients*

Recently, many authors have analyzed radial trends in the SFR (Balogh et al. 1998, 1999; Ellingson et al. 2001) of galaxies in the CNOC1 sample (Yee et al. 1996). Here we investigate what mechanism is responsible for the SFR gradient with the special interests in the effect of the RPS.

In Figure 5 we show median SFRs for observations and our models as a function of projected radius. The observed SFR distribution taken from Diaferio et al. (2001) is indicated by diamonds. The galaxies brighter than $M_R = -20.5$ are selected assuming the same cosmology as our simulations. In this figure we show the low-redshift sample of Diaferio et al. (2001). The data were constructed by superposing seven CNOC1 clusters at the redshift range $0.18 < z < 0.3$. Hereafter, we refer to this superposing sample as the "CNOC sample" in this paper. The details are given in Diaferio et al. (2001) and references therein. We show relative SFRs, which are normalized by the field median value obtained from the same redshift range, because the observed SFRs determined by $W_{\rm O\,II}$ have a lot of uncertainties. For both the observational and simulation data, we exclude the brightest cluster galaxies because they often have quite different properties from other cluster galaxies. The standard, low SFR, and minor burst models are represented in the top, middle, and bottom panels, respectively. Corresponding RPS models are also shown in each panel.

Except for the low SFR model, all our models are broadly consistent with the observation. As expected, the low SFR model has much closer SFR to the field SFR than other models. If we adopt the star formation timescale that reproduces the observed amount of the cold gas in the field galaxies, the difference by the RPS is small compared to the observational errors. While it is interesting that the effect of the RPS can be seen even at $r/R_{200} \sim 1.5$, it should not be overinterpreted when comparing with observations because

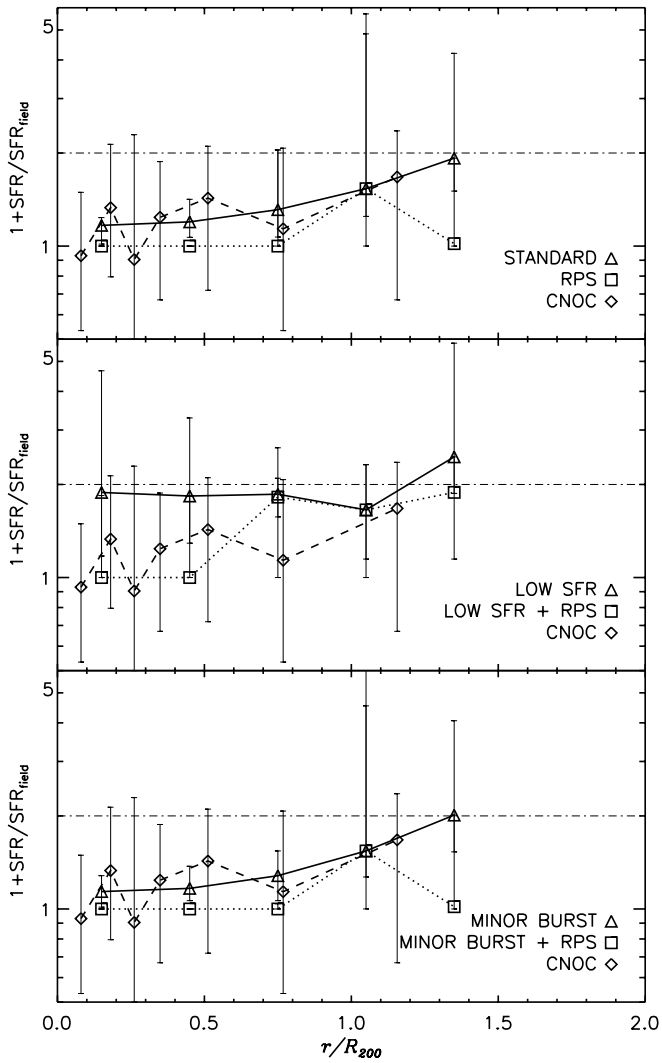

FIG. 5.—Median SFRs of galaxies with $M_R < -20.5$ are plotted as a function of projected radius at $z = 0.2$. Solid lines in the top, middle, and bottom panels show the SFRs in the standard, low SFR, and minor burst models, respectively. The corresponding RPS models are indicated by the dotted lines. The observed median SFR of the galaxies in the CNOC sample is taken from Diaferio et al. (2001) and shown by the asterisks. The dot-dashed line indicates the median SFR in the field model. An error bar shows the 25th to 75th percentile of the distribution in each bin.

the simulated region by the high-resolution particles is spherical, and then the depth of the line of sight at the outermost bin through the high-resolution region is quite thin.

As a result, in our simulation the number of galaxies at the outer regions of the cluster becomes small, and the field contamination is substantially underestimated. For direct comparison with the observations at large radii, we need larger simulations.

We confirm that the minor burst hardly affects the SFR distribution.

4.3. *Color Gradients*

The color of a galaxy reflects the SFR of the galaxy, and it is a more reliable observable than the SFR. It has been known that galaxies in inner regions of clusters are redder than those in outer regions (Butcher & Oemler 1984). Recent observations have confirmed the existence of these color gradients in the galaxy population, which appear to

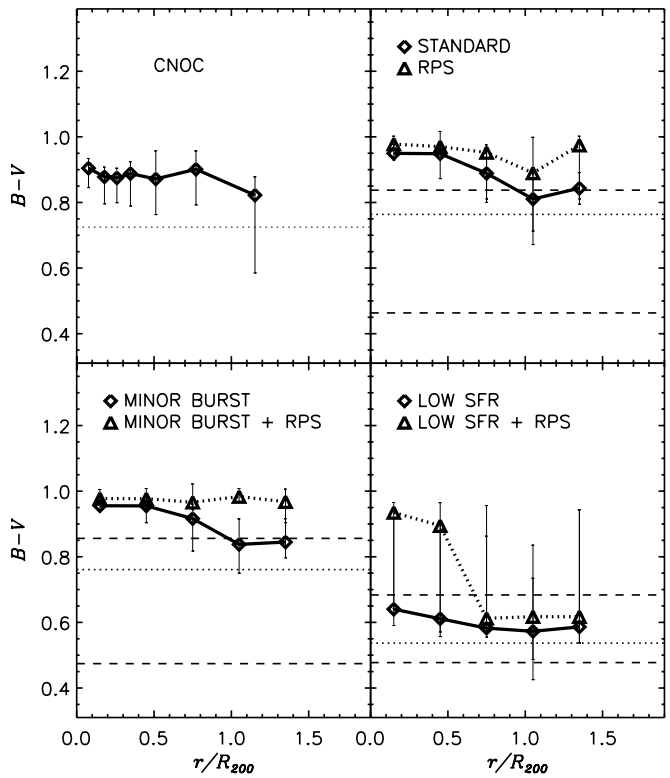

FIG. 6.—Median rest frame $B-V$ colors of cluster galaxies with $M_R < -20.5$ are plotted as a function of projected radius. In the upper left panel, the diamonds denote the observed median colors of the CNOC sample, which are taken form Diaferio et al. (2001). The median color of field galaxies with $M_R < -20.5$ at the same redshift range are shown by the dotted line. The diamonds in the upper right, lower left, and lower right panels indicate the median colors of the galaxies at $z = 0.2$ by the standard, minor burst, and low SFR models as a function of projected radius, respectively. The corresponding RPS model is shown by the triangles in each panel. The median color of the galaxies in the field model with $M_R < -20.5$ at $z = 0.2$ is also shown by the dotted line in each panel. An error bar shows the 25th to 75th percentile of the distribution in each bin. We also show the 25th to 75th percentile of the distribution for the galaxies in the field model by the dashed lines.

continue even beyond the virial radius ($\sim 2R_{200}$; Abraham et al. 1996; Carlberg, Yee, & Ellingson 1997).

In Figure 6 we show the $B-V$ colors of the cluster galaxies as a function of the projected radius at $z = 0.2$. As the observational counterpart, we use the same sample that we used for the SFR gradients. Thus, we use the galaxies brighter than $M_R = -20.5$ again. The median color of field galaxies is shown by dotted lines.

For the standard and minor burst models, the effect of the RPS is more significant at large radii, because, in the central part, the star formation is strongly suppressed by the stripping of the hot gas, regardless of the RPS. Although it is difficult to say whether the models with the RPS show better agreement with the observation because our models are less contaminated by field population as we mentioned previously, the standard/RPS model seems to show too steep/flat gradient compared with the observation. It may suggest that the RPS somewhat affects the color gradients observed in clusters. On the other hand, for the low SFR model, the suppression of the star formation by the stripping of the hot gas is quite weak, and the cluster galaxies have similar colors to the field sample in this model. Then the suppression of the star formation is dominated by the RPS in the low SFR+RPS model. It is found that the effect of the RPS is effective at $r < 0.5R_{200}$. While the minor burst makes galaxies slightly redder than the standard model, the models with and without the minor burst still produces very similar results.

4.4. *Morphology*

Morphologies of cluster galaxies have a strong dependence on their environments and redshifts. Here we investigate how each process affects the morphologies of the model galaxies as functions of projected radius and redshift.

4.4.1. *Morphology Distribution*

Recently, some authors have studied the morphology-density or morphology-radius relations by using a hybrid method of N-body simulations and SA models (Okamoto & Nagashima 2001; Diaferio et al. 2001; Springel et al. 2001). Okamoto & Nagashima and Diaferio et al. concluded that the morphology evolution by only major mergers cannot explain the S0 or intermediate B/T population in clusters, and additional processes are required to understand this population. While Springel et al. seemed to reproduce the observational data of Whitmore et al. (1993), they adopted a wider B/T range for S0 galaxies ($0.096 < \mathrm{B/T} < 0.45$) than the standard classification ($0.4 < \mathrm{B/T} < 0.6$). The small threshold value between spirals and S0 galaxies and wider range of B/T may imply necessity of the additional processes.

One possible process is the RPS of cold gas from a galactic disk (Gunn & Gott 1972; Fujita & Nagashima 1999). According to Fujita & Nagashima, at a central part of a cluster, the SFR of the disk component rapidly drops owing to the RPS, and then the galaxy becomes red and the disk becomes dark. They suggested that a Sb galaxy is turned into a S0 galaxy as a result of the RPS. Another possibility is the minor merger induced bulge formation. Mihos & Hernquist (1994) showed that gas supply to a galaxy center by a minor merger triggers a star burst, and then the galaxy evolves toward the early-type gradually.

Here we examine how these processes affect the morphologies of cluster galaxies by comparing our galaxy populations in the minor burst and RPS models with those in the standard model and the CNOC sample. Since we do not have any information about galaxy morphology in our models except for B/T, we classify the galaxies based on their B/Ts in both our models and the CNOC sample. According to Balogh et al. (1998), we classify galaxies into three classes: a bulge-dominated class, a disk-dominated class, and an intermediate class. In the CNOC sample, Diaferio et al. (2001) have split the galaxy population based on the r-band B/T, and then galaxies with $\mathrm{B/T} > 0.7$ are identified as bulge-dominated galaxies, $\mathrm{B/T} < 0.4$ as disk-dominated galaxies, and $0.4 < \mathrm{B/T} < 0.7$ as intermediate galaxies. We classify our model galaxies based on the B-band B/T. The boundaries between the three classes are chosen so that the morphological fractions in the field models match those of the field galaxies in the CNOC sample. As a result, the galaxies with B-band $\mathrm{B/T} > 0.4$ are identified as bulge-dominated galaxies, $\mathrm{B/T} < 0.25$ as disk-dominated galaxies, and $0.25 < \mathrm{B/T} < 0.4$ as intermediate galaxies in the standard models, and $\mathrm{B/T} > 0.5$ for the bulge-dominated and $\mathrm{B/T} < 0.3$ for the disk-dominated galaxies in the minor burst models.

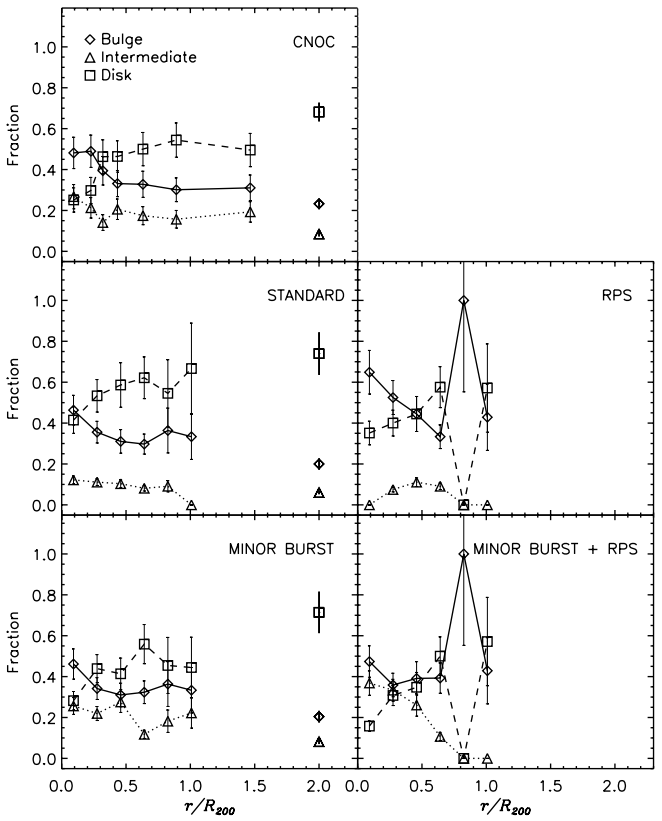

FIG. 7.—Morphological fractions are plotted as a function of projected radius. The diamonds, triangles, and squares indicate the bulge-dominated, intermediate, and disc-dominated fractions, respectively. In the top panel we show the observed fractions for the galaxies with $M_R < -20.5$ in the CNOC sample, which are taken from Diaferio et al. (2001). Other panels show the fractions in the standard, RPS, minor burst, and minor burst+RPS models for the simulated cluster at $z = 0.2$. The symbols at $r/R_{200} = 2$ indicate the fractions in the field in each panel. The error bars present the Poisson errors.

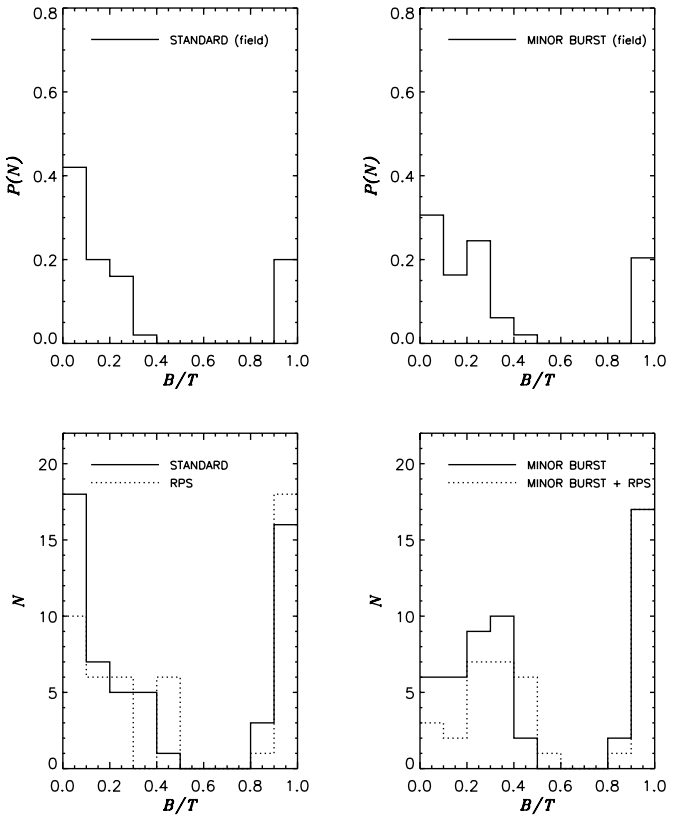

FIG. 8.—Distribution of *B*-band B/T in the field (*upper panels*) and cluster (*lower panels*). we show the probabilistic distribution for the field galaxies and the number distribution for the cluster galaxies. In the lower panels the corresponding RPS modes are also shown by the dotted lines.

The fraction of galaxies with $M_R < -20.5$ in each class is shown in Figure 7 as a function of projected clustercentric radius and that of the field galaxies are shown at $r/R_{200} = 2$ in left panels. By comparison of the CNOC sample with the standard model, it is confirmed that the intermediate fraction in our model is much smaller than the observation, while the bulge-dominated fraction in our model agrees with the observation. This problem has been indicated as a shortcoming of the major merger-induced morphology evolution model (Okamoto & Nagashima 2001; Diaferio et al. 2001).

When we consider the RPS, although the bulge-dominated fraction is increased and the disk-dominated fraction is decreased, the intermediate fraction is still small and it is even decreased at the center. It is because most of the disk-dominated galaxies are almost pure disk galaxies, as we will show, and then the RPS simply darkens the disk-dominated galaxies rather than increasing their B/Ts. Furthermore, the intermediate galaxies with relatively large B/Ts are changed into the bulge-dominated galaxies. The strange behavior seen in the RPS models at $r/R_{200} > 0.7$ results from the small number of galaxies at the radius because of the spherical high-resolution region as we discussed previously. At that radius, all the disk-dominated galaxies become darker than the luminosity cutoff by the RPS by chance. We expect that such behaviors are not observed if we consider field contamination properly and increase the number of clusters. In fact, when we adopt a fainter luminosity cutoff, this behavior is not observed because the number of galaxies is increased.

The minor burst increases the intermediate fraction without changing the bulge-dominated fraction because it affects only galaxies with small bulge-to–total mass ratios. As a result, the minor burst model reproduces the observed fractions quite well despite the fact that it does not influence other properties of galaxies. Now the disk-dominated galaxies tend to be non–pure disk galaxies. Consequently, the RPS can change their B/Ts by the fading of their disks. In the minor burst+RPS model, we can see the increasing intermediate fraction toward the center. It indicates that the disk-dominated galaxies have larger bulges in the inner part of the cluster resulting from the minor burst.

To clarify the effects of the minor burst and RPS, we show B/T distributions for our model galaxies with $M_R < -20.5$ at $z = 0.2$ in Figure 8. The probabilistic number distributions for the field are represented as a function of B/T in top panels. In the standard model, there is a large blank between B/T = 0.4 and 0.9, and the distribution has peaks at B/T $\simeq$ 0 and 1. In the minor burst model the galaxies have similar B/T distribution to that in the standard model, while the peak at B/T $\simeq$ 0 is lowered and the galaxies have slightly extended B/T distribution.

In the lower panels we show the B/T distributions of the galaxies within R_{200} in the standard models (*left*) and the minor burst models (*right*). The models with and without the RPS are indicated by the dotted and solid lines, respec-

tively. To see the influence of the RPS, we do not normalize the distribution by the total number of galaxies.

In the standard model as well as in the field model, the B/T distribution has peaks at B/T $\simeq$ 0 and 1. By comparing the standard model to the RPS model, it is found that the RPS changes the distribution in two ways. First, it decreases the number of galaxies brighter than the luminosity cutoff. Since the RPS only affects the luminosity of the disk component, the number of the disk-dominated galaxies is more easily decreased than the galaxies with large B/Ts. Second, the RPS increases the B/Ts of non–pure disk (and of course non–pure bulge) galaxies. In our case, this effect is the most significant around B/T = 0.4.

In the minor burst model, lower B/T distribution is significantly changed from that in the standard model. The peak at B/T $\simeq$ 0 in the standard model moves to B/T = 0.3–0.4 in the minor burst model. In the cluster, the effect of the minor burst is stronger than in the field because of the higher merger rate. The RPS works in the same way as in the standard model, but now the galaxies in the cluster center have larger bulges than those in the standard model (Fig. 7), and the RPS increases the intermediate B/T fraction in the center.

As we have shown here, the B/T distribution gives us much more useful information than classifying galaxies into three types. Therefore, the direct comparison of the B/T distribution predicted by a model with the observed B/T distributions in various environments will be a crucial test for the morphology evolution model.

4.4.2. *Morphology Evolution*

Dressler et al. (1997) noted that the S0 fraction of cluster galaxies appears to decrease with redshift. Although Andreon (1998) argued that it is difficult to define a reliable S0-E ratio (S0/E), van Dokkum & Franx (2001) pointed out that, in clusters, at least the early-type (E+S0) fraction decreases with redshift. To probe the role of each environmental effect in the morphology evolution, we plot the non–disk-dominated galaxy fractions and the number ratios of the intermediate galaxies to the bulge-dominated galaxies (hereafter Int/Bulge) in the upper and lower panels of Figure 9, respectively. We select the galaxies brighter than $M_R = -20.5$ within $R_{\rm vir}$ at each redshift.

All models show the gradually decreasing non–disk-dominated fractions with redshift. This qualitatively agrees with the observational trend of decreasing early-type fraction in clusters with redshift; however, we cannot make quantitative comparison because the correlation between the Hubble-type and B/T (eq. [5]) has a quite large scatter, and we do not know whether this relation is adequate for cluster galaxies. There is no doubt that the hot gas stripping and the RPS is responsible for the change of the non–disk-dominated fractions. These processes not only increase the B/T of the galaxies but also decrease the number of galaxies brighter than the cutoff luminosity. The latter is also important because the disk-dominated galaxies are more easily darkened by these stripping processes, and then the disk-dominated fraction decreases toward lower redshift.

Our Int/Bulge show completely different trends from the observed S0/E. These ratios are flat or moderately increasing functions of redshift, albeit the observed S0/E is a strongly decreasing function. This feature can be understood from the following reason. In our models the bulges

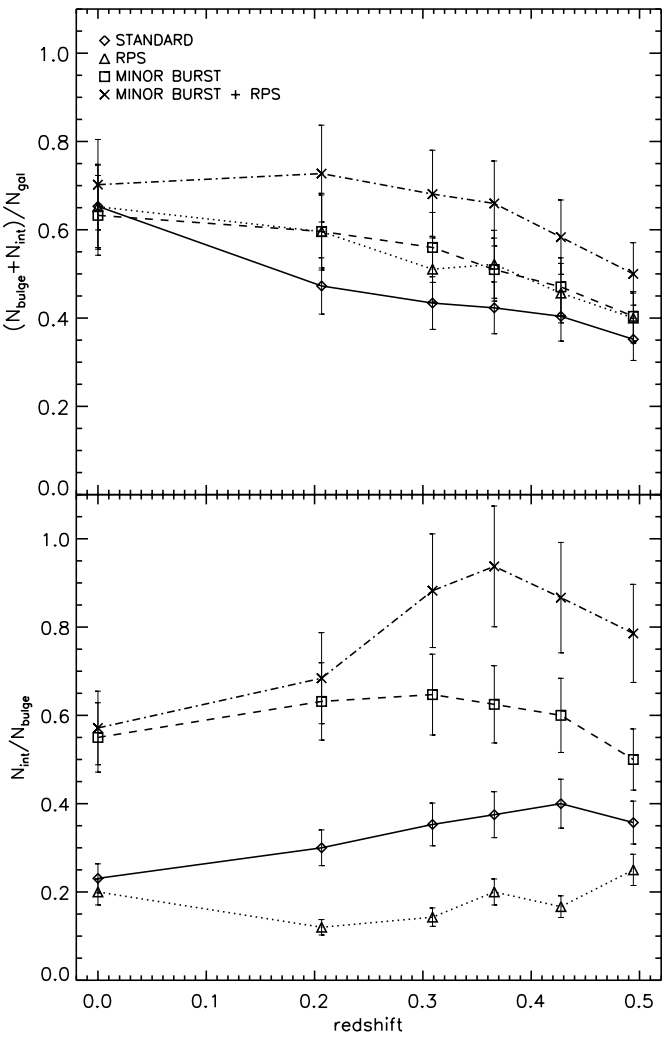

FIG. 9.—*Upper panel*: The non–disk-dominated fractions in the cluster virial radius as a function of redshift. The diamonds, triangles, squares, and crosses indicate the standard, RPS, minor burst, and minor burst+RPS models, respectively. The classification criteria are the same as Fig. 7. *Lower panel*: Int/Bulge as a function of redshift. The error bars present the Poisson errors.

are formed through mergers, and the merger rate is only high before cluster formation. Thus, the bulges hardly grow up in clusters. Hence, the main process that evolves the galaxy morphology in clusters is the fading of disks through gas stripping. As we mentioned above, this process increases B/T (i.e., it increases the bulge-dominated and intermediate galaxies) and darkens the galaxies. As a result, although both the bulge-dominated and intermediate galaxies are increased, the intermediate galaxies are more likely to be darkened and fall below the cutoff luminosity than the bulge-dominated galaxies. Then the Int/Bulge in the cluster become flat or increasing functions of redshift under the merger-driven bulge formation model.

We have to consider the processes that form or evolve bulges in clusters in order to produce an Int/Bulge similar to the observed S0/E. However, it is probably still possible that the Int/Bulge shows different evolution from the S0/E because the eyeball classification does not depend only on the B/T. In fact, the disks of luminous Sa–Sb galaxies are substantially thickened and the spiral features are vanished

by tidal encounters in clusters and they become galaxies resembling S0 galaxies without the large change in their B/Ts (Moore et al. 1999). We expect that observations of the Int/Bulge as a function of redshift will give important information about the formation process and/or epoch of the intermediate B/T population.

5. SUMMARY AND DISCUSSION

In this paper, we have investigated the effects of hot gas stripping, the RPS of cold disk gas, major mergers, and minor mergers on the evolution of bright cluster galaxies, for which the other mechanism, say, galaxy harassment, is probably not the predominant process. We have used a combination of the cosmological *N*-body simulations and the SA galaxy formation model. This method enables us to study the above environmental effects in a fully cosmological context. We have determined the model parameters of the reference model to reproduce observations of nearby field galaxies and CMRs of local cluster elliptical galaxies.

Our main results are summarized as follows:

1. The process that terminates star formation in early-type galaxies is starburst, because the CMRs for early-type galaxies in the cluster are almost independent of either the star formation timescale or the presence of the RPS.
2. If we adopt an appropriate star formation timescale, so as to reproduce the observed cold gas mass fraction in the field, the dominant process that determines colors of galaxies in the cluster core is the stripping of hot gas reservoirs. The effect of the RPS is only substantial when we adopt a much longer star formation timescale.
3. The minor burst does not affect galaxy properties except for morphology.
4. Without the minor burst, galaxies typically separate into almost pure disk ($B/T \simeq 0$) and almost pure bulge ($B/T \simeq 1$) galaxies. The gap in the B/T distribution causes the deficiency of the intermediate B/T galaxies and makes the intermediate galaxy fraction very sensitive to the adopted B/T range. The minor burst decreases the galaxies with $B/T \simeq 0$ and increases those with $B/T = 0.3$–0.4. This effect is larger in the cluster than in the field reflecting a richer merger history, and then the model with the minor burst can reproduce the observed morphology-radius relations.
5. The RPS gives quite small changes in the morphological fractions in the central part of the cluster under the bulge formation only by major mergers. When the minor burst is considered, the disk-dominated galaxies in the cluster center tend to have larger bulges than in the standard model, so that the RPS increases/decreases the intermediate/disk-dominated galaxy fraction there.
6. The fractions of the non–disk-dominated galaxies in the cluster are decreasing functions of redshift. This feature agrees with the observed evolution of early-type fraction in clusters. On the other hand, the Int/Bulge are flat or slightly increasing functions of redshift unlike the observed S0/E.

The stripping of the hot gas from galactic halos suppresses the star formation in the cluster core so efficiently that the effect of RPS is seen only at the outskirts of the cluster. In order to find out this effect observationally, it would be worthwhile to compare the colors or SFRs of the galaxies in cluster outskirts with those of the galaxies lying in regions with the same local density as the cluster outskirts but not associated with clusters. Note that we do not have enough samples at the cluster outskirts, and we underestimate field contamination because of the small volume and spherical shape of the high-resolution region in our simulation. Moreover, we assume instantaneous stripping of cold gas by the RP as a maximal effect, so that we must overestimate the stripping effect. Thus, it would be more difficult to see the difference by RPS in observations.

We have shown that bulge formation solely by major mergers has the difficulty of forming galaxies of intermediate B/T ($\sim$0.3–0.8) in both the field and cluster. The minor burst can resolve this problem because it develops the bulge of the disk-dominated galaxies. This effect is more significant for the cluster galaxies than the field galaxies reflecting richer merger histories. Then the minor burst can reproduce the observed morphology-radius relation. Since the disk-dominated galaxies in clusters tend to have larger bulges than those in the field by the minor burst, this also provides a reasonable answer to the problem that the fading of the disk-dominated galaxies like field spirals cannot explain the entire cluster S0 population as there is too little luminosity density in spiral bulges (e.g., Dressler 1980). When the minor burst is considered, the RPS can increase/decrease the intermediate/disk-dominated galaxy fraction at the cluster center, while the colors and SFRs of these galaxies are hardly changed. Our results show that the minor burst is a very important process that explains morphology evolution of galaxies, although our treatment is too simple. In order to construct a feasible morphology evolution model induced by mergers, the comparison of model predictions and observations in low-density environments (field and groups) where the RPS and the galaxy harassment are not important and the merger is the predominant process that leads morphological transformation will be quite helpful.

In all our models, the bulge formation is driven by mergers, and then the Int/Bulge becomes a flat or slightly increasing function of redshift in contrast to the observed S0/E distribution, whether we include the fading of disks due to the RPS or not. This is because the merger rate is only high before the cluster formation (Okamoto & Habe 1999; Gottlöber, Klypin, & Kravtsov 2001), and the bulges hardly evolve in the cluster. This discrepancy between our models and the observation can be explained by the difference in the classification methods, that is, the Hubble type of galaxy depends on its SFR as well as its B/T. Consequently, star-forming intermediate B/T galaxies could be classified as spirals and non–star-forming disk-dominated galaxies have a chance to be classified as S0 galaxies (Koopman & Kenney 1998). If the Int/Bulge is also observed as a decreasing function of redshift, we will have to consider other bulge formation processes that increase bulge luminosity of the disk-dominated galaxies in high-density environment.

We are grateful to S. Mineshige, Y. Fujita, and T. Kodama for their fruitful comments. Numerical computation in this work was carried out on SGI Origin 2000 at Division of Physics, Graduate School of Science, Hokkaido University and on SGI Origin 3000 at Yukawa Institute Computer Facility.

REFERENCES

Abadi, M. G., Moore, B., & Bower, R. G. 1999, MNRAS, 308, 947
Abraham, R. G., et al. 1996, ApJ, 471, 694
Andreon, S. 1998, ApJ, 501, 533
Andreon, S., & Ettori, S. 1999, ApJ, 516, 647
Balogh, M. L., Morris, S. L., Yee, H. K. C., Carlberg, R. G., & Ellingson, E. 1999, ApJ, 527, 54
Balogh, M. L., Navarro, J. F., & Morris, S. L. 2000, ApJ, 540, 113
Balogh, M. L., Schade, D., Morris, S. L., Yee, H. K. C., Carlberg, R. G., & Ellingson, E. 1998, ApJ, 504, L75
Barnes, J. E. 1996, in ASP Conf. Ser. 92, Formation of the Galactic Halo—Inside and Out, ed. H. L. Morrison & A. Salajedini (San Francisco: ASP), 415
Baugh, C. M., Cole, S., & Frenk, C. S. 1996, MNRAS, 283, 1361
Benson, A. J., Cole, S., Frenk, C. S., Baugh, C. M., & Lacey, C. G. 2000, MNRAS, 311, 793
Bertschinger, E., & Gelb, J. M. 1991, Comput. Phys., 5, 164
Blanton, M., Cen, R., Ostriker, J. P., & Strauss, M. 1999, ApJ, 522, 590
Bond, J. R., Cole, S., Efstathiou, G., & Kaiser, N. 1991, ApJ, 379, 440
Bower, R. G. 1991, MNRAS, 248, 332
Bower, R. G., Lucy, J. R., & Ellis, R. S. 1992, MNRAS, 254, 601
Briel, U. G., Henry, J. P., & Böhringer, H. 1992, A&A, 259, L31
Butcher, H., & Oemler, A. 1978, ApJ, 219, 18
———. 1984, ApJ, 285, 426
Carlberg, R. G., Yee, H. K. C., & Ellingson, E. 1997, ApJ, 478, 462
Cen, R., & Ostriker, J. P. 2000, ApJ, 538, 83
Cole, S., Aragón-Salamanca, A., Frenk, C. S., Navarro, J. F., & Zepf, S. E. 1994, MNRAS, 271, 781
Cole, S., Lacey, C. G., Baugh, C. M., & Frenk, C. S. 2000, MNRAS, 319, 168
Couch, W. J., Barger, A. J., Smail, I. Ellis, R. S., & Sharples, R. M. 1998, ApJ, 497, 188
Davis, M., Efstathiou, G., Frenk, C. S., & White, S. D. M. 1985, ApJ, 292, 371
Diaferio, A., Kauffmann, G., Balogh, M. L., White, S. D. M., Schade, D., & Ellingson, E. 2001, MNRAS, 323, 999
Dressler, A. 1980, ApJ, 236, 351
Dressler, A., et al. 1997, ApJ, 490, 577
Ellingson, E., Lin, H., Yee, H. K. C., & Carlberg, R. G. 2001, ApJ, 547, 609
Folkes, S., et al. 1999, MNRAS, 308, 459
Fujita, Y., & Nagashima, M. 1999, ApJ, 516, 619
Gallagher, J. S., Bushouse, H., & Hunter, D. A. 1989, AJ, 97, 700
Ghigna, S., Moore, B., Governato, F., Lake, G., Quinn, T., & Stadel, J. 1998, MNRAS, 300, 146
Gottlöber, S., Klypin, A., & Kravtsov, A. V. 2001, ApJ, 546, 223
Governato, F., Moore, B., Cen, R., Stadel, J., Lake, G., & Quinn, T. 1997, NewA, 2, 91
Gunn, J. E., & Gott, J. R. 1972, ApJ, 176, 1
Hoffman, Y., & Ribak, E. 1991, ApJ, 380, L5
Huchtmeier, W. K., & Richter, O.-G. 1988, A&A, 203, 237
Impey, C. D., Sprayberry, D., Irwin, M. J., & Bothun, G. D. 1996, ApJS, 105, 209
Katz, N., Hernquist, L., & Weinberg, D. H. 1999, ApJ, 523, 463
Kauffmann, G. 1996, MNRAS, 281, 487
Kauffmann, G., & Charlot, S. 1998, MNRAS, 294, 705
Kauffmann, G., Colberg, J. M., Diaferio, A., & White, S. D. M. 1999, MNRAS, 307, 529
Kauffmann, G., & Haehnelt, M. 2000, MNRAS, 311, 576
Kauffmann, G., White, S. D. M., & Guiderdoni, B. 1993, MNRAS, 264, 201
Kodama, T., & Arimoto, N. 1997, A&A, 320, 41
Kodama, T., Arimoto, N., Barger, A. J., & Aragón-Salamanca, A. 1998, A&A, 334, 99
Kodama, T., & Bower, R. G. 2001, MNRAS, 321, 18
Koopmann, R. A., & Kenney, J. D. P. 1998, ApJ, 497, L75
Lacey, C., & Cole, S. 1993, MNRAS, 262, 627
Larson, R. B., Tinsley, B. M., & Caldwell, C. N. 1980, ApJ, 237, 692
Loveday, J., Peterson, B., Efstathiou, G., & Maddox, S. 1992, ApJ, 390, 338
Mihos, J. C., & Hernquist, L. 1994, ApJ, 425, L13
Moore, B., Katz, N., Lake, G., Dressler, A., & Oemler, A. 1996, Nature, 379, 613
Moore, B., Lake, G., Quinn, T., & Stadel, J. 1999, MNRAS, 304, 465
Nagashima, M., & Gouda, N. 2001, MNRAS, 325, L13
Nagashima, M., Totani, T., Gouda, N., & Yoshii, Y. 2001, ApJ, 557, 505
Nagashima, M., Yoshii, Y., Totani, T., & Gouda, N. 2002, ApJ, 578, 675
Navarro, J. F., Frenk, C. S., & White, S. D. M. 1997, ApJ, 490, 493
Netterfield, C. B., et al. 2002, ApJ, 571, 604
Okamoto, T., & Habe, A. 1999, ApJ, 516, 591
———. 2000, PASJ, 52, 457
Okamoto, T., & Nagashima, M. 2001, ApJ, 547, 109
Pearce, F. R., et al. 1999, ApJ, 521, L99
Press, W. H., & Schechter, P. L. 1974, ApJ, 187, 425
Ratcliffe, A., Shanks, T., Parker, Q., & Fong, R. 1998, MNRAS, 293, 197
Roukema, B. F., Peterson, B. A., Quinn, P. J., & Rocca-Volmerrange, B. 1997, MNRAS, 292, 835
Sandage, A., Binggeli, B., & Tammann, G. A. 1985, AJ, 90, 1759
Simien, F., & de Vaucouleurs, G. 1986, ApJ, 302, 564
Somerville, R. S., & Primack, J. R. 1999, MNRAS, 310, 1087
Somerville, R. S., Primack, J. R., & Faber, S. M. 2001, MNRAS, 320, 504
Springel, V., White, S. D. M., Tormen, G., & Kauffmann, G. 2001, MNRAS, 328, 726
Steinmetz, M., & Müller, E. 1995, MNRAS, 276, 549
Sutherland, R., & Dopita, M. A. 1993, ApJS, 88, 253
Suzuki, T. K., Yoshii, Y., & Beers, T. C. 2000, ApJ, 540, 99
Terlevich, A. I., Caldwell, N., & Bower, R. G. 2001, MNRAS, 326, 1547
Tormen, G. 1997, MNRAS, 290, 411
Totani, T., & Yoshii, Y. 2000, ApJ, 540, 81
van Dokkum, P. G., & Franx, M. 2001, ApJ, 553, 90
van Dokkum, P. G., Franx, M., Kelson, D. D., Illingworth, G. D., Fisher, D., & Fabricant, D. 1998, ApJ, 500, 714
Walker, I. R., Mihos, J. C., & Hernquist, L. 1996, ApJ, 460, 121
Weinberg, D. H., Hernquist, L., & Katz, N. 1997, ApJ, 477, 8
Whitmore, B. C., Gilmore, D. M., & Jones, C. 1993, ApJ, 407, 489
Yee, H. K. C., Ellingson, E., & Carlberg, R. G. 1996, ApJS, 102, 269
Zucca, E., et al. 1997, A&A, 326, 477